Fluorogenic and genetic targeting of a red-emitting molecular calcium indicator

Sylvestre Bachollet, Nicolas Pietrancosta, Jean-Maurice Mallet, Blaise Dumat

COMMUNICATION

Fluorogenic and Genetic Targeting of a Red-Emitting Molecular Calcium Indicator

Received 00th January 20xx,
Accepted 00th January 20xx

DOI: 10.1039/x0xx00000x

Sylvestre P.J.T. Bachollet,[a] Nicolas Pietrancosta,[a,b] Jean-Maurice Mallet[a] and Blaise Dumat[a]*

We introduce a strategy for the fluorogenic and genetic targeting of a calcium indicator by combining a protein fluorogen with the BAPTA sensing group. The resulting dual-input probe acts like a fluorescent AND logic gate with a Ca^{2+}-sensitive red emission that is activated only upon reaction with HaloTag with a 25-fold intensity enhancement and can be used for wash-free calcium imaging in Hela cells. The modular all-molecular design relying on a well-estalished protein self-labeling tag opens future possibilitie for tuning the photophysical properties or target different analytes.

To decipher biological processes of increasing complexity using fluorescence imaging, the development of "smart" probes able to report on biological analytes or processes with good selectivity and appropriate spatial and temporal resolutions is crucial. Ca^{2+} imaging is used extensively by biologists as an indirect measure of the electrical activity of cells to follow neuronal communication. It is a complex endeavor since it aims at recording localized and transient concentration spikes and is a typical example where sophisticated probes are required.[1] Calcium probes essentially fall into two categories: (i) Genetically-encoded calcium indicators (GECIs) based on fluorescent proteins[2] and (ii) molecular fluorescent calcium probes.[3–5] Currently, the field is dominated by GECIs, owing to the ability to selectively express them in a chosen cell type or sub-cellular compartment.[2]

The genetic targeting of small chemical indicators using self-labeling protein tags (SLP tags) has emerged as a promising strategy to combine the selectivity of GECIs with the diversity of molecular probes.[6–8] The most commonly used SLP tags, SNAP-tag and HaloTag, have for instance been used to control the subcellular localization of Ca^{2+} or Zn^{2+} probes.[9–12] However, even with an efficient targeting reaction, one has to get rid of the unbound probes that may yield an unspecific signal. Metal cations sensors often involve cell-impermeant carboxylate chelating groups masked as ester functions and the excess of dye cannot always be easily washed away after esterase hydrolysis in cells. One way to circumvent this issue is to use fluorogenic targeting where the fluorescence is only activated upon binding to a target protein.[13,14] Although there is large body of work on the development of single-input fluorogenic reporters for high-contrast protein imaging (Figure 1A),[15–17] there are much fewer instances of fluorogenic activation of chemical sensors via protein binding. The fluorogenic protein targeting of a functional chemical probe indeed makes for a difficult molecular design, since it requires the combination of two fluorescence activating mechanisms (fluorogenic protein reaction AND analyte sensing ability, Figure 1B) that may work well independently but lose efficiency when nested within the same molecule. Lavis and coworkers coupled a HaloTag-targeted fluorogenic Si-rhodamine probe with the calcium chelator BAPTA.[18] Once coupled to BAPTA, it afforded a far-red targetable calcium indicator, but the probe lost most of its fluorogenic character with only a 2.4-fold increase in intensity upon reaction with HaloTag. To build-up hybrid fluorogenic and chemogenetic indicators, researchers have thus resorted to alternative strategies where the analyte detection is achieved via the protein moiety[19,20] or using a two-step labeling reaction involving a fluorogenic tetrazine ligation[21] but the combination of fluorogenic protein targeting and analyte sensing within the same molecular probe has only rarely been achieved with satisfying results.[22]

[a] *Laboratoire des biomolécules, LBM, Département de chimie, École normale supérieure, PSL University, Sorbonne Université, CNRS, 75005 Paris, France..*
[b] *Neuroscience Paris Seine - Institut de Biologie Paris Seine (NPS - IBPS) INSERM, CNRS, Sorbonne Université, Paris, France.*

† Footnotes relating to the title and/or authors should appear here.
Electronic Supplementary Information (ESI) available: [details of any supplementary information available should be included here]. See DOI: 10.1039/x0xx00000x

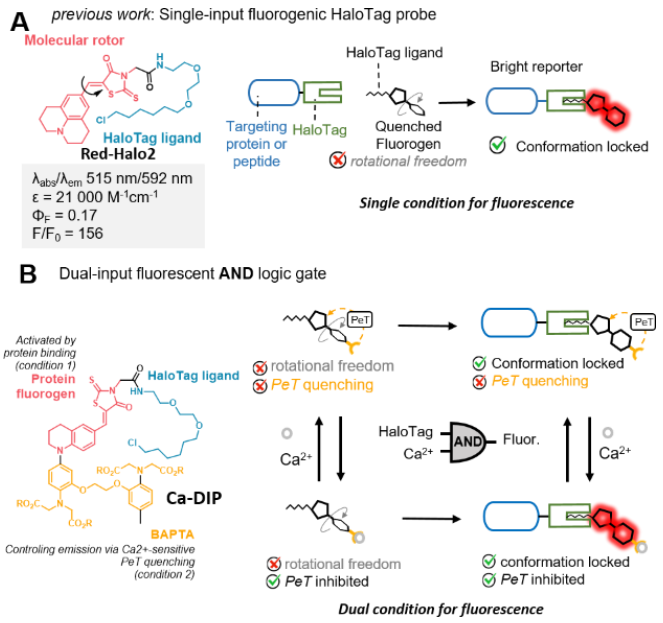

Figure 1. Design of the dual-input calcium probe **Ca-DIP**. (A) previously reported fluorogenic HaloTag probe Red-Halo2 and general principle of fluorogenic protein targeting. (B) Structure of Ca-DIP and general design principle of the fluorescent AND logic gate dually activated by HaloTag and Ca^{2+}.

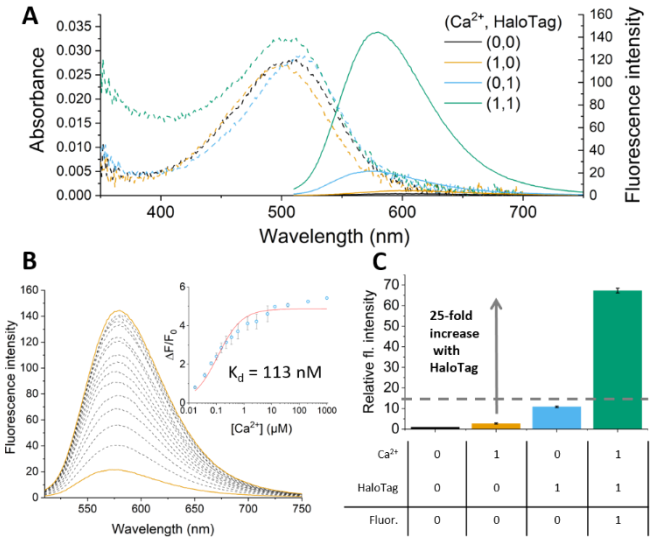

Figure 2. in vitro characterization of Ca-DIP. (A) Absorption (dashed lines) and emission (full lines) spectra of Ca-DIP in the presence (39 μM) or absence (0 μM) of Ca^{2+} in the free and HaloTag bound form ([Ca-DIP] = 1 μM, λ_{exc} = 500 nm). (B) Calcium titration of HaloTag bound Ca-DIP from 0 to 1000 μM Ca^{2+}. Inset graph shows the signal expressed as $\Delta F/F_0$ where F_0 is the initial fluorescence at 0 μM Ca^{2+} (average of two measurements). To calculate the dissociation constant, the titration was fitted to a hill function (n = 1) shown in red. (C) Logic gate operation and truth table of Ca-DIP as a function of Ca^{2+} and HaloTag. Integrated intensities F normalized to the intensity F_0 of the free probe in the absence of Ca^{2+} and HaloTag (average of two measurements). Input states 0 and 1 correspond to 0 μM Ca^{2+} and 39 μM Ca^{2+} or to the free and HaloTag-bound probe respectively. An arbitrary intensity limit (dashed line) can be set to distinguish between 0 (low) and 1 (high) output.

In this work, we have set out to combine a fluorogenic molecular rotor scaffold with the calcium sensing group BAPTA to build the hybrid chemogenetic and fluorogenic probe **Ca-DIP** (**Ca**lcium **D**ual-**I**nput **P**robe) with a dual-input emission in the red range activated by reaction with the protein self-labeling tag HaloTag and by binding to Ca^{2+} cations (Figure 1B). Such a dually-conditioned probe can be described as a fluorescent AND logic gate where the target analytes are the inputs and the fluorescence signal is the output.[23] The structure of **Ca-DIP** is built on **Red-Halo2**, a fluorogenic HaloTag probe that we recently developed based on a dipolar molecular rotor structures with a viscosity-sensitive emission (Figure 1A).[16,24] Upon reaction with HaloTag, its broad orange-red emission is enhanced 156-fold. The polarity and viscosity-sensitive fluorescence emission is an inherent feature of a wide variety of flexible dipolar structures,[25] which made us confident that we could make large structural modifications to transform **Red-Halo2** into a chemical sensor without losing the protein fluorogenicity. To obtain a dual-input probe with calcium sensitivity (**Ca-DIP**), the structure of **Red-Halo2** was redesigned to incorporate a BAPTA moiety (Figure 1B). BAPTA is the common calcium chelator developed by Tsien on which the vast majority of molecular calcium probes such as Fura-2 or Oregon green BAPTA is built.[3–5,26] When non-electronically coupled to a fluorophore, it quenches the fluorescence emission by photoinduced electron transfer (PeT). Calcium binding inhibits the PeT process and thus restores the fluorescence, creating an on/off switch actuated by Ca^{2+} cations. **Red-Halo2** was built on a julolidine electron-rich group, since the locked aniline derivative inhibits the formation of a twisted intramolecular charge transfer (TICT) which results in higher brightness.[16] Since the efficiency of PeT is directly related to the distance between the electron donor and acceptor groups, we seeked to position the BAPTA moiety in close proximity to the **Red-Halo2** scaffold. Replacing the julolidine of **Red-Halo2** by a tetrahydroquinoline had the benefit to maintain the inhibition of TICT while offering a reactive amine function to incorporate the BAPTA moiety (scheme S1).

The optical properties of **Ca-DIP** were first characterized *in vitro* to study its fluorescent response to HaloTag and calcium. **Ca-DIP** free in Ca^{2+}-free buffer displays a broad absorption band centered on 508 nm with an absorptivity of 33 000 $M^{-1}{\cdot}cm^{-1}$ and a very weak fluorescence emission (Figure 2A and Table S1 for detailed photophysical properties). The addition of calcium to the free or HaloTag bound probe induces a small hypsochromic shift of the absorption wavelength confirming that the BAPTA is only weakly conjugated to the fluorophore, which is a condition for an efficient PeT process. The addition of calcium is expected to inhibit the PeT-quenching but, thanks to the dual activation, Ca^{2+} alone induces only a minute increase of fluorescence intensity. On the other hand, **Ca-DIP** becomes fluorescent upon reaction with HaloTag with a 25-fold increase in intensity and exhibits a Ca^{2+}-sensitive emission (Figure 2).

In agreement with the rational design, the fluorescence of **Ca-DIP** is thus simultaneously controlled by two external inputs and it operates a fluorescent AND logic gate able to sense calcium only when bound to the HaloTag protein (Figure 2C). The calcium sensing ability was further studied by performing a calcium titration of **Ca-DIP** bound to HaloTag. **Ca-DIP** displays a 6.4-fold increase of fluorescence intensity from 0 μM to 1 mM

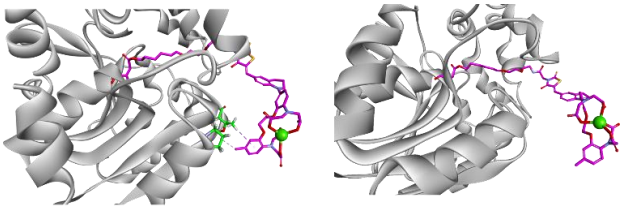

Cluster 1: 74 % of conformations
E_{pot} = -223 791 kJ.mol^{-1}

Cluster 2: 26 % of conformations
E_{pot} = -223 698 kJ.mol^{-1}

Figure 3. Molecular dynamics of Halo-Tag-bound Ca-DIP. Representative structures of the two clusters of conformations of Ca-DIP bound to Ca^{2+} and HaloTag obtained by molecular dynamics.

Ca^{2+} and a dissociation constant K_d of 113 nM (Figure 2B). This affinity ranks it among high affinity calcium indicators and is due to the substitution of the BAPTA with an electron-rich amine. Ca-DIP thus exhibits very promising Ca^{2+}-sensing properties that are comparable to those of alternative fluorogenic and chemogenetic calcium indicators, but with an all-molecular approach (Table S2). However, its fluorescence brightness is markedly lower than that of the parent compound **Red-Halo2** (Table S1). To try to understand this drop in intensity, we studied the binding of **Ca-DIP** to HaloTag by molecular dynamics. **Ca-DIP** complexed with Ca^{2+} was covalently attached to the HaloTag crystal structure and we performed a 2 ns dynamic with a 10 ps step, generating 200 conformations. A cluster analysis underlined the presence of two representative structures accounting for 74 % and 26 % of the conformations (Figure 3). In the minor cluster, **Ca-DIP** does not interact with the protein and adopts a planar conformation suitable for fluorescence emission. In the major cluster, the methyl group of BAPTA is found to interact with a hydrophobic pocket formed by Proline 259, Threonine 252 and Alanine 260 on the surface of HaloTag. These hydrophobic interactions successfully minimize the potential energy of the complex but they twist the molecule in a non-planar conformation unfavorable for fluorescence that may explain the limited brightness of **Ca-DIP** compared to the parent compound **Red-Halo2**.

To test the probe in cellular imaging, we synthesized an acetoxymethyl (AM) ester analogue **Ca-DIP-AM**, following the classical strategy used for making calcium probes cell permeant (Scheme S1). We assessed the ability of the probes to record localized calcium concentration variations following Histamine stimulation in Hela cells transiently expressing HaloTag fusion proteins. In non-excitable cells, Histamine is known to induce an

increase in cytoplasmic calcium concentration with periodic oscillations.[27] We first imaged cells expressing a soluble HaloTag protein. The dye was incubated for 60 min leaving the time for cell permeation and AM ester hydrolysis and time-course imaging over 5 minutes was performed (Figure S1 and SI movie 1). The addition of Histamine induced an enhancement of the fluorescence intensity consistent with an increase in cytosolic calcium (Figure S1C). The monitoring of non-transfected cells (cell #4 and #5 on Figure S1B) showed no significant fluorescence signal and no variation over the course of the experiment (Figure S1D).

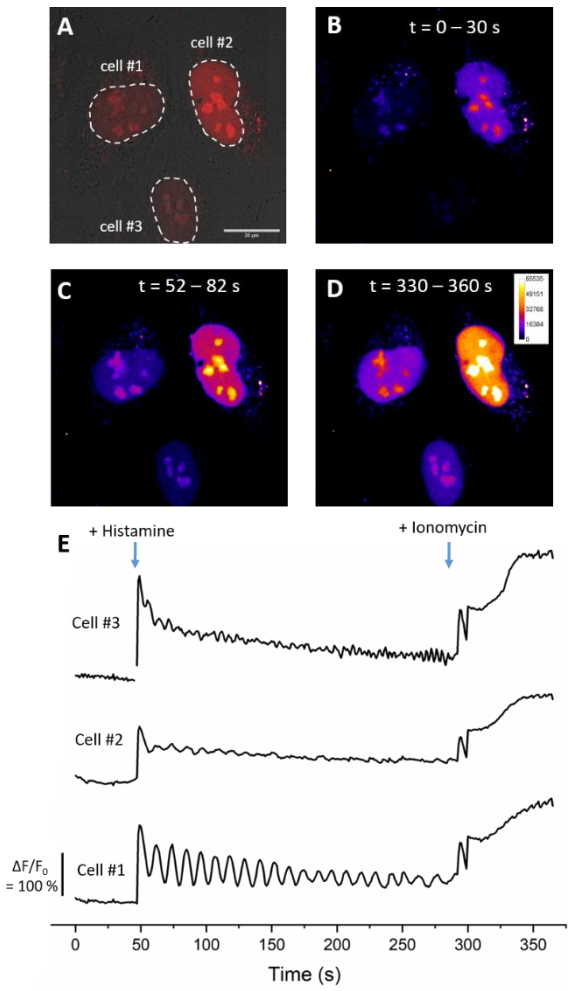

Figure 4. Calcium imaging of Hela cells transfected with HaloTag-NLS and incubated with 1 µM of Ca-DIP-AM. Time-lapse imaging at 1 frame/s. Histamine (50 µM) was added at 50 s and ionomycin/Ca^{2+} (5 µM/10 mM) at 290 s. (A) Average intensity projection fluorescence image merged with the transmission image showing cell numbering. (B,C,D) Intensiometric images obtained by averaging 30 frames before addition of histamine (B), after addition of histamine (C) and after addition of ionomycin (D). (E) Evolution of the average intensity in the nucleus of the cells numbered on panel (A) over the course of the experiment, plotted as a percentage of variation relative to the initial intensity $\Delta F/F_0$.

To further evidence the ability of our probes to selectively image calcium in genetically-defined organelles, we performed a similar experiment in cells expressing a nuclear HaloTag-NLS protein (Figure 4 and SI movie 2). The average intensity projection image shows a clear selective staining of the nucleus even without a washing protocol (Figure 4A). The average intensity measured in the nucleus of 3 different cells shows a clear increase of the fluorescence signal (from 140 to 250 %) following histamine stimulation at 50 s with periodic oscillation visible for one cell with good temporal resolution (Figure 4B, C&E). To determine the maximum fluorescence enhancement in the cellular environment, ionomycin and calcium were then added at 290 s (Figure 4D&E). Ionomycin is a calcium transporter that will saturate the cell in calcium ions and allow Ca-DIP to reach its maximum fluorescence

enhancement values that vary between 210 and 400 %. Although we observe a clear selective staining of the nucleus (Figure 4A), it is inevitable to observe some nonspecific signal due to the off-target activation of the probe in hydrophobic regions of the cells. We have thus also monitored the signal intensity in cytoplasmic regions of cells #1 to #3 (Figure 4 and Figure S2). The low nonspecific signal does not show any sensitivity to calcium concentration changes showing that the binding to the target HaloTag protein is necessary to activate the calcium-sensitive emission of the probe. Despite having a moderate sensitivity to calcium *in vitro* (F/F_0 = 6.4), the cellular performance of the probe in cells is quite satisfactory, allowing targeted calcium imaging with a maximum signal increase up to 400 % that is comparable or superior to the performance of recently reported BAPTA-based or chemogenetic calcium indicators in similar experiments (Figure 4C, Table S2).[19,28,29]

In conclusion, we have successfully used a fluorogenic molecular scaffold targeting HaloTag to develop one of the first fluorescent molecular logic gate for genetically targeted calcium imaging. With the help of molecular dynamics calculations, combined molecular and protein engineering can be envisioned to optimize the properties of the sensor/protein complex and in particular its brightness. The versatile design strategy described herein allows future tuning of the fluorescence properties[24] and application to other analytes and/or to different proteins by selecting the proper sensing moieties and ligands. It may thus open many new possibilities for localized functional imaging in genetically-defined cell types or subcellular organelles.

There are no conflicts to declare

This work was supported by the Agence Nationale de la Recherche (ANR-18-CE44-0006).

Notes and references

1 C. Grienberger and A. Konnerth, *Neuron*, 2012, **73**, 862–885.

2 B. Podor, Y. Hu, M. Ohkura, J. Nakai, R. Croll and A. Fine, *Neurophotonics*, 2015, **2**, 021014.

3 M. Oheim, M. van 't Hoff, A. Feltz, A. Zamaleeva, J.-M. Mallet and M. Collot, *Biochim. Biophys. Acta - Mol. Cell Res.*, 2014, **1843**, 2284–2306.

4 J. T. Lock, I. Parker and I. F. Smith, *Cell Calcium*, 2015, **58**, 638–648.

5 R. Y. Tsien, *Biochemistry*, 1980, **19**, 2396–2404.

6 C. A. Hoelzel and X. Zhang, *ChemBioChem*, 2020, **21**, 1935–1946.

7 G. V. Los, L. P. Encell, M. G. McDougall, D. D. Hartzell, N. Karassina, C. Zimprich, M. G. Wood, R. Learish, R. F. Ohana, M. Urh, D. Simpson, J. Mendez, K. Zimmerman, P. Otto, G. Vidugiris, J. Zhu, A. Darzins, D. H. Klaubert, R. F. Bulleit and K. V. Wood, *ACS Chem. Biol.*, 2008, **3**, 373–382.

8 A. Keppler, S. Gendreizig, T. Gronemeyer, H. Pick, H. Vogel and K. Johnsson, *Nat. Biotechnol.*, 2003, **21**, 86–9.

9 M. L. Zastrow, Z. Huang and S. J. Lippard, *ACS Chem. Biol.*, 2020, **15**, 396–406.

10 M. Kamiya and K. Johnsson, *Anal. Chem.*, 2010, **82**, 6472–6479.

11 M. Bannwarth, I. R. Corrêa, M. Sztretye, S. Pouvreau, C. Fellay, A. Aebischer, L. Royer, E. Ríos and K. Johnsson, *ACS Chem. Biol.*, 2009, **4**, 179–190.

12 R. Liu, T. Kowada, Y. Du, Y. Amagai, T. Matsui, K. Inaba and S. Mizukami, *ACS Sensors*, 2022, **7**, 748–757.

13 C. Li, A. Tebo and A. Gautier, *Int. J. Mol. Sci.*, 2017, **18**, 1473.

14 M. P. Bruchez, *Curr. Opin. Chem. Biol.*, 2015, **27**, 18–23.

15 L. Wang, M. Tran, E. D'Este, J. Roberti, B. Koch, L. Xue and K. Johnsson, *Nat. Chem.*, 2020, **12**, 165–172.

16 S. P. J. T. Bachollet, C. Addi, N. Pietrancosta, J.-M. Mallet and B. Dumat, *Chem. – A Eur. J.*, 2020, **26**, 14467–14473.

17 J. B. Grimm, A. K. Muthusamy, Y. Liang, T. A. Brown, W. C. Lemon, R. Patel, R. Lu, J. J. Macklin, P. J. Keller, N. Ji and L. D. Lavis, *Nat. Methods*, 2017, **14**, 987–994.

18 C. Deo, S.-H. Sheu, J. Seo, D. E. Clapham and L. D. Lavis, *J. Am. Chem. Soc.*, 2019, **141**, 13734–13738.

19 A. G. Tebo, F. M. Pimenta, M. Zoumpoulaki, C. Kikuti, H. Sirkia, M. A. Plamont, A. Houdusse and A. Gautier, *ACS Chem. Biol.*, 2018, **13**, 2392–2397.

20 C. Deo, A. S. Abdelfattah, H. K. Bhargava, A. J. Berro, N. Falco, H. Farrants, B. Moeyaert, M. Chupanova, L. D. Lavis and E. R. Schreiter, *Nat. Chem. Biol.*, 2021, **17**, 718–723.

21 J. J. Gruskos, G. Zhang and D. Buccella, *J. Am. Chem. Soc.*, 2016, **138**, 14639–14649.

22 T. Fujii, Y. Shindo, K. Hotta, D. Citterio, S. Nishiyama, K. Suzuki and K. Oka, *J. Am. Chem. Soc.*, 2014, **136**, 2374–2381.

23 A. Romieu, *Org. Biomol. Chem.*, 2015, **13**, 1294–1306.

24 S. P. J. T. Bachollet, Y. Shpinov, F. Broch, H. Benaissa, A. Gautier, N. Pietrancosta, J.-M. Mallet and B. Dumat, *Org. Biomol. Chem.*, in press , DOI:10.1039/D1OB02394B.

25 A. S. Klymchenko, *Acc. Chem. Res.*, 2017, **50**, 366–375.

26 M. Collot, C. D. Wilms, A. Bentkhayet, P. Marcaggi, K. Couchman, S. Charpak, S. Dieudonné, M. Häusser, A. Feltz and J.-M. Mallet, *Elife*, 2015, **4**, 1–18.

27 G. Dupont and L. Combettes, *F1000Research*, , DOI:10.12688/F1000RESEARCH.8438.1.

28 H. Ogasawara, M. Grzybowski, R. Hosokawa, Y. Sato, M. Taki and S. Yamaguchi, *Chem. Commun.*, 2018, **54**, 299–302.

29 K. Hirabayashi, K. Hanaoka, T. Egawa, C. Kobayashi, S. Takahashi, T. Komatsu, T. Ueno, T. Terai, Y. Ikegaya, T. Nagano and Y. Urano, *Cell Calcium*, 2016, **60**, 256–265.